Theory of Quantum Plasmon Resonances in Doped Semiconductor Nanocrystals

ARTICLE *in* THE JOURNAL OF PHYSICAL CHEMISTRY C · JULY 2014

Impact Factor: 4.77 · DOI: 10.1021/jp5046035

THE JOURNAL OF PHYSICAL CHEMISTRY C

Article

pubs.acs.org/JPCC

Theory of Quantum Plasmon Resonances in Doped Semiconductor Nanocrystals

Hui Zhang,*[,†] Vikram Kulkarni,[‡] Emil Prodan,[§] Peter Nordlander,[‡] and Alexander O. Govorov*[,†]

[†]Department of Physics and Astronomy, Ohio University, Athens, Ohio 45701, United States

[‡]Department of Physics and Astronomy, M.S. 61, Rice University, Houston, Texas 77005, United States

[§]Department of Physics, Yeshiva University, New York, New York 10016, United States

Supporting Information

ABSTRACT: Doped semiconductor nanocrystals represent a new type of quantum plasmonic material with optical resonances in the infrared. These nanocrystals are fundamentally different from the metal nanoparticles because the electron density in a semiconductor can be tuned over a wide interval. Using the DFT-based time-dependent formalism, we computed the absorption spectra of doped quantum dots as a function of the number of carriers in the dot. The dynamic properties of doped quantum dots undergo an interesting transition from the size-quantization regime to the classical regime of plasmon oscillations. We demonstrated this quantum-to-classical transition for both self-doped copper chalcogenide dots and impurity-doped II−VI nanocrystals. We also showed that the plasmon frequency and electron density in the dot depend on the type of doping, which can be bulk-like or surface-like. The results obtained in this study can be used to predict and describe optical properties of a variety of semiconductor nanocrystals with quantum plasmonic resonances.

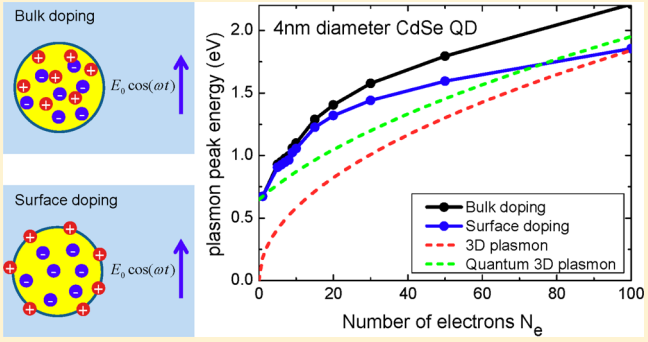

INTRODUCTION

The ability to tune the electron density in semiconductor quantum dots (QDs) is a very attractive property since it allows us to change the optical responses of nanocrystals and, in particular, the frequency of their collective plasmon oscillations.[1−3] This is in drastic contrast to the traditional metal nanocrystals with a high and almost unchangeable density of electrons.[4,5] Semiconductor QDs can be self-doped by introducing vacancies into the crystal lattice; this type of doping has been presently well developed for copper chalcogenide QDs, $Cu_{2-x}Y$ with Y = S, Se, or Te.[1−3,6−18] In such nanocrystals, the density of mobile holes in the valence band increases with increasing the vacancy parameter x. More traditionally doped QDs are realized with the II−V and II−VI semiconductors such as CdS, ZnSe, CdSe, InAs, InP, and ZnO.[19−27] In these QDs the doping is done by incorporating various types of impurities into the crystal lattice. Another type of doping was developed in the papers.[27−29] In this case, the doping mechanism arises from the photocharging effect which involves electron transfer from molecules adsorbed on the surface of the QD.

While the optical properties of moderately doped semiconductor QDs are strongly influenced by quantum confinement effects, the plasmon resonances of metal nanoparticles are typically described by classical electromagnetic approaches. Recently several studies have highlighted significant quantum effects in plasmonic systems and contributed to the development of the novel field of quantum plasmonics.[30,31] Several time-dependent density functional theory (DFT) studies have demonstrated significant differences between quantum-mechanical and classical descriptions of plasmon resonances in nanoparticles.[32−36] Nonlocal corrections of the dielectric function designed to describe the Fermi-pressure effects in an electron gas have also recently been developed and found to qualitatively agree with experimental data.[37−40] Recent experimental studies have demonstrated a blue shift of plasmon resonances in small Ag nanoparticles[41] and electron tunneling mediated charge transfer plasmons in nanoparticle dimers with subnanometer gaps.[42,43] It has been shown that the confinement of carriers in metal nanoparticles leads to the collisional size-dependent decay of plasmons.[44] In colloidal photodoped QDs, the transition from the quantum size-quantization regime to the classical plasmonic picture with increasing number of carriers has been observed experimentally and described theoretically within the Lorentz oscillator model.[27] Quantum effects in plasmonics also appear in hybrid nanocrystal complexes that exhibit the effects of exciton−plasmon interaction between a two-level quantum system (a dot or molecule) and a metal nanoparticle.[45−55]

Received: May 9, 2014
Revised: June 23, 2014
Published: June 27, 2014

dx.doi.org/10.1021/jp5046035 | J. Phys. Chem. C 2014, 118, 16035−16042

In this paper, we investigate optical properties and collective excitations of doped QDs using the DFT-based time-dependent formalism. With increasing number of carriers in a QD, we observe a transition from purely quantum-mechanical single-electron excitations to quantum-plasmonic excitations and eventually to classical collective plasmon oscillations. This quantum-to-classical transition is unique for semiconductor nanocrystals and seems impossible for metals because the electron density in a plasmonic metal nanoparticle is typically large and challenging to control. We demonstrate this type of physics for two families of QDs that are self-doped copper chalcogenide dots and impurity-doped II−VI nanocrystals. Concrete examples of QDs to be considered in this paper include $Cu_{2-x}S$, $Cu_{2-x}Se$, CdSe, and CdS. In the first section we will define theoretical models and methods, whereas the second and third sections will focus on specific material systems such as $Cu_{2-x}Y$ and II−VI QDs.

1. Models of Doped QDs Based on $Cu_{2-x}S$, $Cu_{2-x}Se$, and CdSe. Here we employ the jellium model with a local dielectric constant along with the effective-mass approximation to describe the quantum states and intraband dynamics of the mobile carriers in a semiconductor (Figure 1). In our model, a

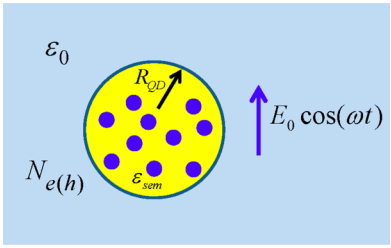

Figure 1. Model of a spherical semiconductor quantum dot embedded into a dielectric matrix (liquid or polymer). The quantum dot is filled with carriers (electrons or holes) and experiences an external electromagnetic field.

QD embedded in a dielectric matrix contains $N_{e(h)}$ particles, which can be either electrons or holes. We first use the DFT and local density approximation (LDA) procedures to compute the electronic ground state.[56,57] Then we continue with the time-dependent LDA (TDLDA) method,[58−60] which is based on the random phase approximation (RPA), and compute absorption spectra of nanocrystals. In application to the metal nanocrystals in a dielectric matrix, such computational methods have been developed in refs 32−34, and the details of the formalism can be found in the Supporting Information.

Our model treats the potential inside a QD as a smooth potential due to a uniform positive background and, therefore, ignores the discreteness of impurities or vacancies. The treatment is well justified for QDs with many electrons that efficiently screen the impurity potential (CdSe QDs) and also for a QD with a large density of positively charged vacancies (copper chalcogenide nanocrystals) when a delocalized carrier feels an averaged potential in a QD. For small numbers of carriers/impurities, our model can only provide a qualitative description, but it still reveals the basic physics of collective excitations in quantum confined systems. In particular, it is of fundamental interest to investigate the quantum dynamics of plasmons in confined systems and to describe the crossover from the size-quantization regime to the regime of classical plasmon oscillations. To demonstrate these effects, we choose three particular material systems, $Cu_{2-x}S$, $Cu_{2-x}Se$, and CdSe, which have been intensively studied over the last years.[1−3,6−17,19,21−24]

We start with the case of $Cu_{2-x}S$ QDs. The material parameters for $Cu_{2-x}S$, taken from the handbook[61] and also the papers,[2,17] are $m_{h,eff} = 0.8m_0$ and $\varepsilon_{sem} = 11.56$, where $m_{h,eff}$ and ε_{sem} are the effective mass of the carriers and the local dielectric constant of semiconductor, respectively. For $Cu_{2-x}Se$ QDs, the parameters are slightly different, $m_{h,eff} = 0.5m_0$ and $\varepsilon_{sem} = 11$. In the dielectric model, the surrounding matrix is a solution with $\varepsilon_0 = 2.25$ which is a typical number in experiments.[2,10] For the size of the QDs, we take the radius of $R_{QD} = 2.5$ nm which is typical for experiments.[1] Furthermore, the numerical TDLDA formalism (see Supporting Information) involves the phenomenological broadening parameter γ and the QD potential depth U_{QD}. Since we are mainly interested in the position of quantum plasmonic resonance, we set the phenomenological broadening parameter γ small (0.04 eV). This will lead to narrow, well-defined peaks in the calculated absorption spectrum of a single QD. The potential depth for the hole potential (U_{QD}) is roughly the energy separation between the top of the valence band of a QD and the HOMO level of the matrix. In our calculations, we simply make the hole potential sufficiently deep ($U_{QD} = -6$ eV) that the hole wave function and the absorption spectra do not change.

We now discuss the levels of doping of $Cu_{2-x}S$ and $Cu_{2-x}Se$ QDs. $Cu_{2-x}S$ is a semiconductor with no free holes at room temperature, whereas CuS is a conductor. When we introduce a deficiency of Cu atoms, a $Cu_{2-x}S$ crystal acquires holes in the valence band. The current literature reports several studies on $Cu_{2-x}S$ QDs;[2,17] the hole concentrations for these systems reported so far are $n_h = 0.77-1.7 \times 10^{21}$ cm^{-3} for $1.93 < 2 - x < 2$ and $n_h = 0.98 \times 10^{22}$ cm^{-3} for $x = 1$ (CuS). For QDs with a radius of $R_{QD} = 2.5$ nm, the corresponding numbers of carriers are $N_h = 50-600$. If we assume that one molecular unit of CuS donates one hole to the valence band, the maximum density of holes in this material is calculated as $n_h = \rho_{CuS} \cdot M_{CuS} = 3 \times 10^{22}$ cm^{-3}, where ρ_{CuS} is the mass density of CuS. Therefore, the maximum number of holes in $Cu_{2-x}S$ QDs is expected to be $N_h \sim 2000$ which would correspond to the case $x = 1$. For $Cu_{2-x}Se$ QDs, we expect similar numbers. In this study, we will compute collective resonances in $Cu_{2-x}S$ and $Cu_{2-x}Se$ QDs for the following range of hole numbers, $1 \leq N_h < 1200$, which covers the current experimental data and also extends toward higher levels of doping.

Regarding n-doped CdSe QDs, this material system has stronger size quantization since the effective mass of electron in CdSe is relatively light, $m_{e,eff} = 0.11m_0$. The dielectric constant of CdSe and the QD radius used in the calculations are $\varepsilon_{sem} = 6.25$ and $R_{QD} = 2$ nm, respectively. The depth of crystal potential of CdSe QDs is given by the affinity of the bulk semiconductor, $U_{QD} = -4.6$ eV. We will see in the following that the quantum effects in the n-type CdSe QDs are much stronger compared to those in the p-type $Cu_{2-x}S$ and $Cu_{2-x}Se$ nanocrystals, which is due to the small effective mass of electrons in CdSe.

2. Absorption Spectra of p-Type $Cu_{2-x}S$ and $Cu_{2-x}Se$ QDs: Quantum and Classical Plasmons. Figure 2 shows the DFT-calculated densities of the ground state of $Cu_{2-x}S$ QDs for various numbers of permanent hole carriers. We see the transition from the few-particle regime with a strongly nonuniform density ($N_h \sim 1-10$) to the many-particle regime with strong screening and a nearly flat carrier density ($N_h \sim 1200$). The absorption spectrum of a doped QD within the

dx.doi.org/10.1021/jp5046035 | J. Phys. Chem. C 2014, 118, 16035−16042

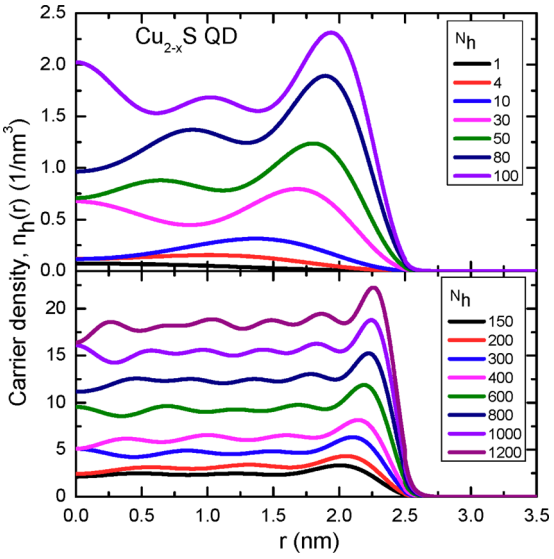

Figure 2. DFT-calculated ground state densitites of $Cu_{2-x}S$ QDs for various numbers of permanent hole carriers in the interval $1 \leq N_h \leq 1200$; $R_{QD} = 2.5$ nm.

DFT-TDLDA approach exhibits a single peak due to a collective mode (Figure 3). As expected, the integrated area of the peak monotonically increases with the number of particles in a QD. It is interesting to look at the position of the peak and compare it with the quantum and classical plasmon dispersions (Figure 4).

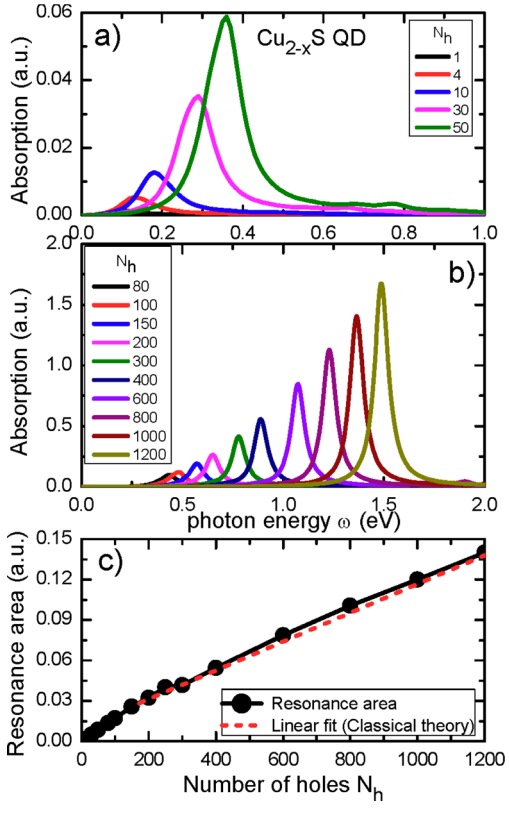

Figure 3. (a) and (b) Calculated optical absorption spectra of $Cu_{2-x}S$ QDs for various numbers of holes. (c) Integrated intensity of the plasmon peak as a function of N_h. The linear fit comes from the classical theory described in the main text.

First, we compare our results with the classical Mie theory of a small plasmonic nanosphere.[62] The absorption of light is given by the polarizability of the QD

$$Q = 2\omega\varepsilon_0 E_0^2 \cdot \mathrm{Im}\,\alpha_{QD}(\omega), \qquad \alpha_{QD}(\omega) = a_{QD}^3 \frac{\varepsilon_{QD}(\omega) - \varepsilon_0}{\varepsilon_{QD}(\omega) + 2\varepsilon_0} \tag{1}$$

where E_0 is the electric-field amplitude of incident light. The local dielectric function of a semiconductor is given by

$$\varepsilon_{QD}(\omega) = \varepsilon_{sem} - \frac{\omega_{p,bulk}^2}{\omega(\omega + i\gamma)}, \qquad \omega_{p,bulk}^2 = \frac{4\pi e^2 n_h(N_h)}{m_h^*}$$

The density of holes in the above equations is given by $n_h = N_h/V_{QD}$, where V_{QD} is the QD volume. In these equations, $\omega_{p,bulk}$ is the bulk plasmon frequency in a semiconductor. The absorption has a pole at the plasmon resonance frequency of the QD

$$Q \sim \mathrm{Im}\,\frac{1}{\varepsilon_{QD}(\omega) + 2\varepsilon_0} \sim \mathrm{Im}\,\frac{1}{\omega - \omega_{p,QD} + i\gamma/2}$$

where the plasmon frequency of the QD is given by

$$\omega_{p,QD} = \frac{\omega_{p,bulk}}{\sqrt{\varepsilon_{sem} + 2\varepsilon_0}} \tag{2}$$

Apparently, $\omega_{p,QD} \to 0$ as $N_h \to 0$, but the calculated collective mode frequency does not approach zero for small carrier numbers because of the size quantization in a QD. A phenomenological fit to the numerical data for the plasmon frequency can be performed using:

$$\omega_{qp} = \sqrt{\omega_{p,QD}^2 + \Delta_{sp}^2} \tag{3}$$

where Δ_{sp} is the optical excitation energy of a spherical QD with one hole ($N_h = 1$) which corresponds to the transition from the s- to p-state. The resulting eq 3 reproduces the single-electron limit. Equation 3 gives the quantum-plasmon frequency and is an attempt to correct the classical plasmon frequency incorporating the size-quantization effect. Note that the formula 3 resembles the equation for intersubband plasmon in 2D-doped semiconductor quantum wells;[63,64] such plasmon modes have been well studied in the past using absorption and inelastic light scattering. Thus, for the few-particle regime we see clearly the quantum effects (Figure 4). Within the classical regime where the number of carriers is large, the calculated plasmon energy is in good agreement with the bulk plasmon frequency $\omega_{p,QD}$ given by eq 2. To obtain even better agreement, we varied R_{QD} slightly and introduced an effective QD radius $R_{QD,eff}$. The effective QD radii shown in Figure 4 are slightly smaller than the geometrical QD radius since the electron density in a QD is nonuniform.

The crossover between the quantum and classical regimes occurs when

$$\omega_{p,QD} \sim \Delta_{sp} \tag{4}$$

We note that plasmon and quantization energies vary differently with the QD size:

$$\Delta_{sp} \propto \frac{\hbar^2}{m_h^* R_{QD}^2}, \qquad \omega_{p,QD} \propto \sqrt{\frac{N_h}{R_{QD}^3}} \tag{5}$$

dx.doi.org/10.1021/jp5046035 | J. Phys. Chem. C 2014, 118, 16035−16042

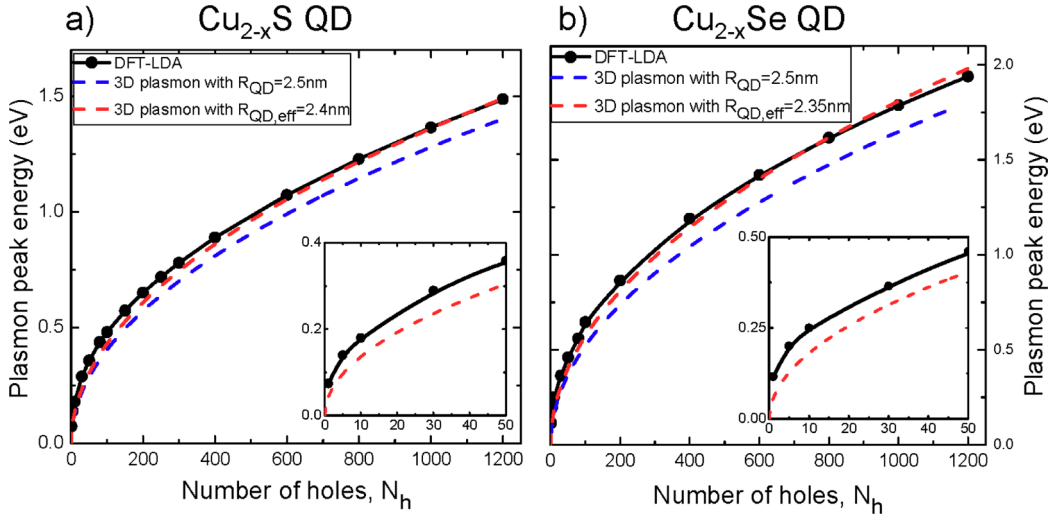

Figure 4. Calculated energy of the collective plasmon peak in the absorption spectra as a function of the number of holes for $Cu_{2-x}S$ (a) and $Cu_{2-x}Se$ QDs (b). The graphs also show the classical and quantum plasmon dispersions given by the formulas in the main text. The insets give the quantum parts of the dispersion of the collective mode at relatively small N_h; the QD radius used in calculations is R_{QD} = 2.5 nm.

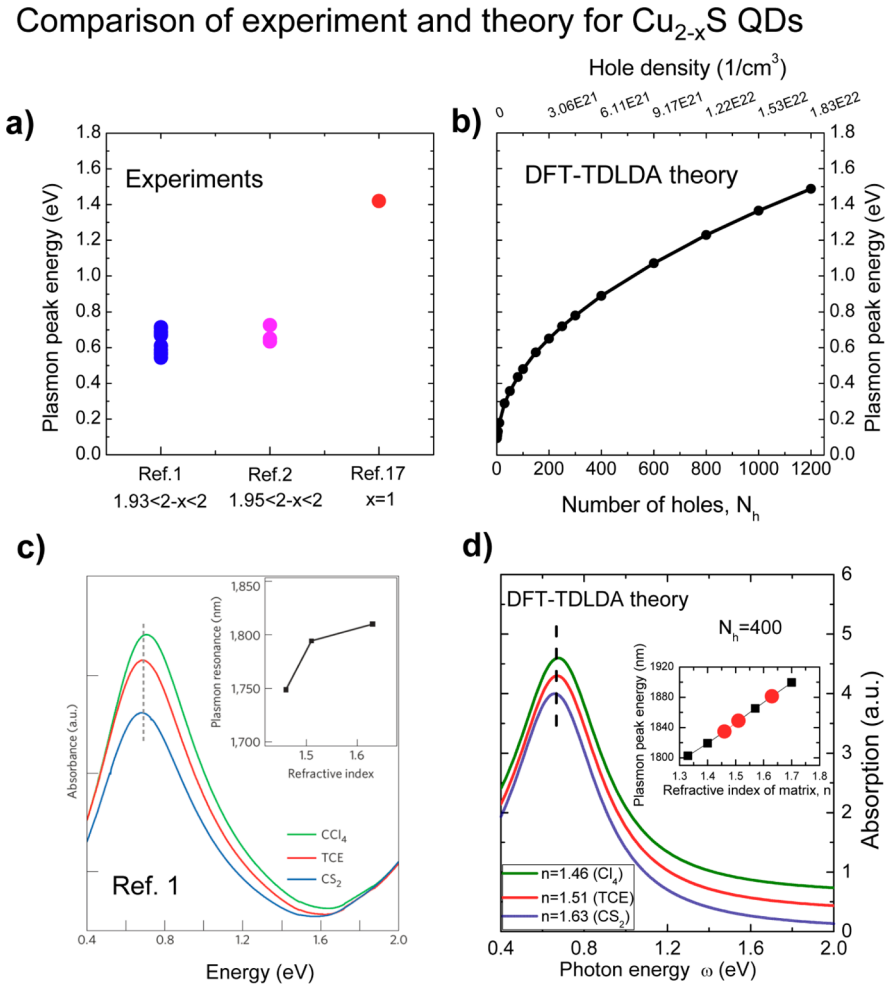

Figure 5. (a) and (b) Measured and calculated positions of the plasmon peak in $Cu_{2-x}S$ QDs. The experimental data were taken from three papers.[2,9,17] The exact concentrations of holes in these experiments are not known and usually estimated from the plasmon energy. The graph (b) depicts the DFT-calculated plasmon energy as a function of hole concentration. (c) and (d) Measured and calculated absorption spectra in different solvents with different refractive indices (1.46, 1.51, and 1.63). In the theoretical plots (d), we set the broadening parameter to be 0.4 eV. The insets show the plasmon wavelength as a function of the refractive index of solvent. In the inset of graph (d), we show the plasmon wavelength for several values of refractive index, but for the experimental values of refractive index, we use red dots. Figure (c) is reproduced with permission from ref 1.

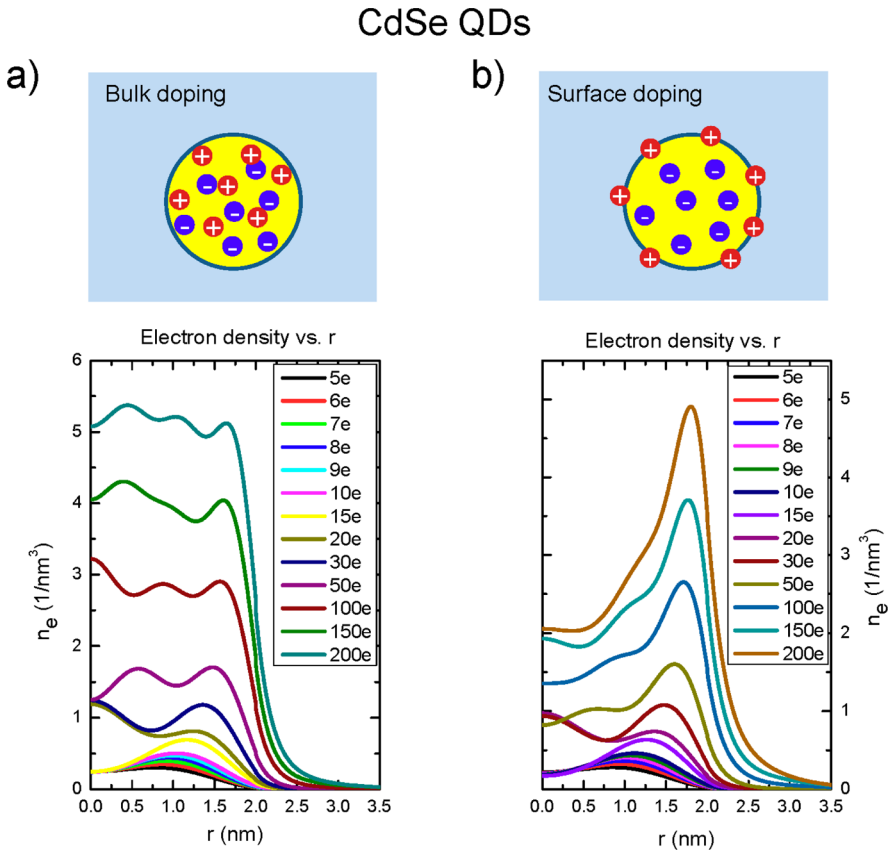

Figure 6. (a) and (b) Models of doping of semiconductor QDs and their densities. As a model system, we take CdSe QDs.

Regarding the strength of the plasmon peak, the classical eq 5 gives

$$I_{\mathrm{pl}} = \int \mathrm{d}\omega \cdot Q(\omega) \sim \omega_{\mathrm{p,QD}}^2 \sim N_{\mathrm{h}}$$

In Figure 3c we show the integrated area of plasmon resonance where the linear fit works well, indicating that our DFT-based calculations are in good agreement with classical theory (eq 5).

The DFT-TDLDA method is applicable for quantum systems with a relatively large number of carriers. For a QD with just a few particles, the TDLDA-calculated energy of a carrier has a significant contribution from the Coulomb self-interaction in the KS equations. Therefore, we do not show in Figure 4 the collective TDLDA data for small numbers $N_{\mathrm{h}} = 1-4$ but add the point for $N_{\mathrm{h}} = 1$ that is the single-particle transition energy calculated from the single-particle Hamiltonian. We see that the DFT results for the many-electron regime and the single-particle energy for the case $N_{\mathrm{h}} = 1$ form one smooth curve in the insets of Figure 4. Overall, the calculated quantum energies are consistently above the classical plasmon dispersions (insets in Figure 4) and approach finite values for a small numbers of holes. These properties are the direct manifestations of quantum plasmonic excitations in QDs with small numbers of carriers.

In the following we compare our data with the available experimental results for $Cu_{2-x}S$ QDs. Figure 5 summarizes some of the experimental observations. First, we choose a reasonable range of concentrations of holes and determine the corresponding numbers of holes in a QD for $1 \leq N_{\mathrm{h}} < 1200$ (see the discussion in Section 1). For these concentrations, our calculations well reproduce the interval of the observed plasmon frequencies (Figure 5a,b). The plasmon frequency is sensitive to the dielectric environment. Figure 5c and 5d present experimental[1] and theoretical data for the QDs in different solvents. The refractive indices of the three solvents used in the experimental paper[1] are 1.46, 1.51, and 1.63. As expected, the plasmon-peak wavelength increases with increasing refractive index $n_0 = \sqrt{\varepsilon_0}$. In the theoretical graph (Figure 5d), we show the experimental values for refractive index with bold dots. Again, we see overall good agreement between the DFT theory and the experiments.

3. Quantum Plasmons and Optical Properties of n-Type CdSe QDs. We expect that quantum effects will be stronger for this material system because of the lighter effective mass of the electrons. The method of incorporation of free carriers into a QD can be bulk or surface doping. In the case of surface doping, electrons come from a donor molecule adsorbed at the surface,[28,29] and an activation of electrons from the surface molecules requires illumination by light. Physically, we expect that the surface doping will create a more nonuniform carrier density compared with bulk doping. Figure 6 shows the carrier densities for the two types of doping. We indeed observe that the surface-doping case exhibits strongly nonuniform density distributions of carrier. This is due to the distribution of impurity charges. The mobile electrons in a QD tend to screen the surface charges and therefore the density of electrons peaks at the QD boundary. For the bulk-doping case, we observe the opposite: The electron density is more uniform since the impurities are everywhere inside a QD, and the electrons tend to uniformly screen these distributed impurities.

Next we show the data for plasmon resonance energies calculated with the time-dependent DFT method (Figure 7).

dx.doi.org/10.1021/jp5046035 | J. Phys. Chem. C 2014, 118, 16035−16042

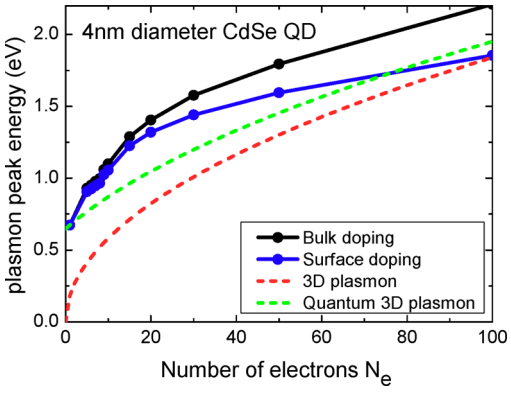

Figure 7. DFT-calculated energy of the collective plasmon peak in the absorption spectra as a function of the number of electrons in CdSe QDs with bulk and surface doping. The graph also shows the classical and quantum plasmon dispersions given by the formulas in the text: R_{QD} = 2.0 nm.

The calculated absorption spectra exhibit a single plasmon peak coming from the dipole excitation mode. For the case N_e = 1, we again calculated the transition energy from the single-particle Hamiltonian. For the many-particle regime, the calculated positions of the dipolar mode are in reasonable agreement with the classical theory for large numbers N_e (Figure 7). For small numbers of electrons, we observe strong deviations from the classical theory which indicate the appearance of quantum effects. The main evidence for the quantum regime is the behavior of the plasmon energy for small electron numbers: the energy of the quantum plasmonic mode does not approach zero. Overall, we see clearly in Figure 7 the transition from the purely quantum regime to the classical regime of plasmon oscillations as the number of electrons increases. As expected, the quantum effects in the plasmonic spectra of CdSe QDs are stronger compared to those in copper chalcogenide QDs. It is also interesting to notice that the plasmon energy in the surface-doped QDs is lower than that for the bulk-doped QDs. This can be explained from the electron densities plotted in Figure 6. In the surface-doped QDs, the electron density in the bulk of QD is relatively small which leads to weaker electric currents across an optically excited QD. Therefore, the plasmon resonance frequency is expected to be lower, and this was indeed observed in our numerical calculations. We also performed similar calculations for CdS QDs which have a slightly heavier effective electron mass (Supporting Information). The CdS QDs also exhibit strong quantum effects in the plasmonic spectra in the limit of small electron populations. Overall, our calculations demonstrate the appearance of the quantum-to-classical transition in plasmonic spectra of several materials. This indicates that the quantum plasmonic regime in doped QDs is a general phenomenon and experimentally observable.

CONCLUSIONS

In this paper, we have investigated the transition between the quantum and classical regimes in the dynamics of doped semiconductor QDs. The quantum effects dominate in QDs with a small number of carriers, whereas heavily doped nanocrystals demonstrate nearly classical plasmon resonances. In our calculations, the frequency of the collective resonance of doped QDs can be tuned with the number of carriers and with the dielectric environment. The results can be used to predict and understand optical properties of a broad class of quantum nanostructures with tunable plasmonic resonances.

ASSOCIATED CONTENT

Supporting Information

Details of DFT-TDLDA formalism and electron density of the CdS QD in the ground state and plasmon resonance energies. This material is available free of charge via the Internet at http://pubs.acs.org.

AUTHOR INFORMATION

Corresponding Authors

*(H.Z.) E-mail: yiaimer@gmail.com.
*(A.O.G.) E-mail: govorov@phy.ohiou.edu.

Notes

The authors declare no competing financial interest.

ACKNOWLEDGMENTS

A.O.G. thanks Daniel Gamelin for motivating discussions. This study was supported by the U.S. Army Research Office under the grant number W911NF-12-1-0407 (H.Z., P.N., and A.O.G.), the Volkswagen Foundation (H.Z. and A.O.G), and the Robert A. Welch Foundation under grant C-1222 (V.K. and P.N.). Use of the Center for Nanoscale Materials was supported by the U.S. Department of Energy, Office of Science, Office of Basic Energy Sciences, under Contract No. DE-AC02-06CH11357.

REFERENCES

(1) Luther, J. M.; Jain, P. K.; Ewers, T.; Alivisatos, A. P. Localized, Surface Plasmon Resonances Arising from Free Carriers in Doped Quantum Dots. *Nat. Mater.* **2011**, *10*, 361−366.
(2) Kriegel, I.; Jiang, C.; Rodríguez-Fernández, J.; Schaller, R. D.; Talapin, D. V.; da Como, E.; Feldmann, J. Tuning the Excitonic and Plasmonic Properties of Copper Chalcogenide Nanocrystals. *J. Am. Chem. Soc.* **2012**, *134*, 1583−1590.
(3) Dorfs, D.; Härtling, T.; Miszta, K.; Bigall, N. C.; Kim, M. R.; Genovese, A.; Falqui, A.; Povia, M.; Manna, L. Reversible Tunability of the Near-Infrared Valence Band Plasmon Resonance in Cu2-xSe Nanocrystals. *J. Am. Chem. Soc.* **2011**, *133*, 11175−11180.
(4) Maier, S. A. *Plasmonics: Fundamentals and applications*; Springer: N.Y., 2007.
(5) Boltasseva, A.; Atwater, H. A. Low-Loss Plasmonic Metamaterials. *Science* **2011**, *331*, 290−291.
(6) Li, S.; Wang, H.; Xu, W.; Si, H.; Tao, X.; Lou, S.; Du, Z.; Li, L. S. Synthesis and Assembly of Monodisperse Spherical Cu2S Nanocrystals. *J. Colloid Interface Sci.* **2009**, *330*, 483−487.
(7) Hsu, S.-W.; On, K.; Tao, A. R. Localized Surface Plasmon Resonances of Anisotropic Semiconductor Nanocrystals. *J. Am. Chem. Soc.* **2011**, *133*, 19072−19075.
(8) Hsu, S.-W.; Bryks, W.; Tao, A. R. Effects of Carrier Density and Shape on the Localized Surface Plasmon Resonances of Cu2_xS Nanodisks. *Chem. Mater.* **2012**, *24*, 3765−3771.
(9) Kruszynska, M.; Borchert, H.; Bachmatiuk, A.; Rümmeli, M. H.; Büchner, B.; Parisi, J.; Kolny-Olesiak, J. Size and Shape Control of Colloidal Copper(I) Sulfide Nanorods. *ACS Nano* **2012**, *6*, 5889−5896.
(10) Kriegel, I.; Rodríguez-Fernández, J.; Wisnet, A.; Zhang, H.; Waurisch, C.; Eychmüller, A.; Dubavik, A.; Govorov, A. O.; Feldmann, J. Shedding Light on Vacancy-Doped Copper Chalcogenides: Shape-Controlled Synthesis, Optical Properties, and Modeling of Copper Telluride Nanocrystals with Near-Infrared Plasmon Resonances. *ACS Nano* **2013**, *7*, 4367−4377.
(11) Scotognella, F.; Della Valle, G.; Srimath Kandada, A. R.; Dorfs, D.; Zavelani-Rossi, M.; Conforti, M.; Miszta, K.; Comin, A.;

Korobchevskaya, K.; Lanzani, G.; et al. Plasmon Dynamics in Colloidal Cu2_xSe Nanocrystals. *Nano Lett.* **2011**, *11*, 4711−4717.
(12) Zhao, Y.; Burda, C. Development of Plasmonic Semiconductor Nanomaterials with Copper Chalcogenides for a Future with Sustainable Energy Materials. *Energy Environ. Sci.* **2012**, *5*, 5564−5576.
(13) Routzahn, A. L.; White, S. L.; Fong, L.-K.; Jain, P. K. Plasmonics with Doped Quantum Dots. *Isr. J. Chem.* **2012**, *52*, 983−991.
(14) Scotognella, F.; Valle, G. D.; Kandada, A. R. S.; Zavelani-Rossi, M.; Longhi, S.; Lanzani, G.; Tassone, F. Plasmonics in Heavily-Doped Semiconductor Nanocrystals. *Eur. Phys. J. B* **2013**, *86*, 154.
(15) Zhao, Y.; Pan, H.; Lou, Y.; Qiu, X.; Zhu, J.; Burda, C. Plasmonic Cu_{2-x} S Nanocrystals: Optical and Structural Properties of Copper-Deficient Copper(I) Sulfides. *J. Am. Chem. Soc.* **2009**, *131*, 4253−4261.
(16) Ma, G.; Zhou, Y.; Li, X.; Sun, K.; Liu, S.; Hu, J.; Kotov, N. A. Self-Assembly of Copper Sulfide Nanoparticles into Nanoribbons with Continuous Crystallinity. *ACS Nano* **2013**, *7*, 9010−9018.
(17) Xie, Y.; Carbone, L.; Nobile, C.; Grillo, V.; D'Agostino, S.; Sala, F. D.; Giannini, C.; Altamura, D.; Oelsner, C.; Kryschi, C.; et al. Metallic-like Stoichiometric Copper Sulfide Nanocrystals: Phase- and Shape-Selective Synthesis, Near-Infrared Surface Plasmon Resonance Properties, and Their Modeling. *ACS Nano* **2013**, *7* (8), 7352−7369.
(18) Faucheaux, J. A.; Stanton, A. L. D.; Jain, P. K. Plasmon Resonances of Semiconductor Nanocrystals: Physical Principles and New Opportunities. *J. Phys. Chem. Lett.* **2014**, *5* (6), 976−985.
(19) Shim, M.; Guyot-Sionnest, P. n-type colloidal semiconductor nanocrystals. *Nature* **2000**, *407*, 981−983.
(20) Erwin, S. C.; Zu, L.; Haftel, M. I.; Efros, A. L.; Kennedy, T. A.; Norris, D. J. Doping semiconductor nanocrystals. *Nature* **2005**, *436*, 91−94.
(21) Norris, D. J.; Efros, A. L.; Erwin, S. C. Doped Nanocrystals. *Science* **2008**, *319*, 1776−1779.
(22) Sahu, A.; Kang, M. S.; Kompch, A.; Notthoff, C.; Wills, A. W.; Deng, D.; Winterer, M.; Frisbie, C. D.; Norris, D. J. Electronic impurity doping in CdSe nanocrystals. *Nano Lett.* **2012**, *12* (5), 2587−2594.
(23) Tuinenga, C.; Jasinski, J.; Iwamoto, T.; Chikan, V. In situ observation of heterogeneous growth of CdSe quantum dots: Effect of indium doping on the growth kinetics. *ACS Nano* **2008**, *2* (7), 1411−1421.
(24) Roy, S.; Tuinenga, C.; Fungura, F.; Dagtepe, P.; Chikan, V. Progress toward producing n-type CdSe quantum dots: Tin and indium doped CdSe quantum dots. *J. Phys. Chem. C* **2009**, *113*, 13008−13015.
(25) Mocatta, D.; Cohen, G.; Schattner, J.; Millo, O.; Rabani, E.; Banin, U. Heavily Doped Semiconductor Nanocrystal Quantum Dots. *Science* **2011**, *332*, 77−81.
(26) Xie, R.; Peng, X. Synthesis of Cu-doped InP nanocrystals (d-dots) with ZnSe diffusion barrier as efficient and color-tunable NIR emitters. *J. Am. Chem. Soc.* **2009**, *131*, 10645−10651.
(27) Schimpf, A. M.; Thakkar, M.; Gunthardt, C. E.; Masiello, D. J.; Gamelin, D. R. Charge-Tunable Quantum Plasmons in Colloidal Semiconductor Nanocrystals. *ACS Nano* **2014**, *8*, 1065−1072.
(28) Ochsenbein, S. T.; Feng, Y.; Whitaker, K. M.; Badaeva, E.; Liu, W. K.; Li, X.; Gamelin, D. R. Charge-Controlled Magnetism in Colloidal Doped Semiconductor Nanocrystals. *Nat. Nanotechnol.* **2009**, *4*, 681−687.
(29) Cohn, A. W.; Janßen, N.; Mayer, J. M.; Gamelin, D. R. Photocharging ZnO Nanocrystals: Picosecond Hole Capture, Electron Accumulation, and Auger Recombination. *J. Phys. Chem. C* **2012**, *116*, 20633−20642.
(30) Tame, M. S.; McEnergy, K. R.; Özdemir, S. K.; Lee, J.; Maier, S. A.; Kim, M. S. Quantum Plasmonics. *Nat. Phys.* **2013**, *9*, 329−340.
(31) Jacob, Z.; Shalaev, V. M. Plasmonics Goes Quantum. *Science* **2011**, *334*, 463−464.
(32) Zuloaga, J.; Prodan, E.; Nordander, P. Quantum Description of the Plasmon Resonances of a Nanoparticle Dimer. *Nano Lett.* **2009**, *9*, 887−891.
(33) Prodan, E.; Nordlander, P. Electronic structure and polarizability of metallic nanoshells. *Chem. Phys. Lett.* **2003**, *352*, 140−146.
(34) Prodan, E.; Nordlander, P.; Halas, N. J. Electronic Structure and Optical Properties of Gold Nanoshells. *Nano Lett.* **2003**, *3*, 1411−1415.
(35) Esteban, R.; Borisov, A. G.; Nordlander, P.; Aizpurua, J. Bridging Quantum and Classical Plasmonics with a Quantum-Corrected Model. *Nat. Commun.* **2012**, *3*, 825.
(36) Townsend, E.; Bryant, G. W. Plasmonic Properties of Metallic Nanoparticles: The Effects of Size Quantization. *Nano Lett.* **2012**, *12*, 429−434.
(37) Ciraci, C.; Hill, R. T.; Mock, J. J.; Urzhumov, Y.; Fernandez-Dominguez, A. I.; Maier, S. A.; Pendry, J. B.; Chilkoti, A.; Smith, D. R. Probing the ultimate limits of plasmonic enhancement. *Science* **2012**, *337*, 1072−1074.
(38) García de Abajo, F. J. Nonlocal Effects in the Plasmons of Strongly Interacting Nanoparticles, Dimers, and Waveguides. *J. Phys. Chem. C* **2008**, *112*, 17983−17987.
(39) Toscano, G.; Raza, S.; Yan, W.; Jeppesen, C.; Xiao, S.; Wubs, M.; Jauho, A.-P.; Bozhevolnyi, S. I.; Mortensen, N. A. Nonlocal response in plasmonic waveguiding with extreme light confinement. *Nanophotonics* **2013**, *2* (3), 161−166.
(40) David, C.; García de Abajo, F. J. Spatial Nonlocality in the Optical Response of Metal Nanoparticles. *J. Chem. Phys.* **2011**, *115*, 19470−19475.
(41) Scholl, J. A.; Koh, A. L.; Dionne, J. A. Quantum Plasmon Resonances of Individual Metallic Nanoparticles. *Nature* **2012**, *483*, 421−427.
(42) Savage, K. J.; Hawkeye, M. M.; Esteban, R.; Borisov, A. G.; Aizpurua, J.; Baumberg, J. J. Revealing the quantum regime in tunnelling Plasmonics. *Nature* **2012**, *491*, 574−577.
(43) Scholl, J. A.; García-Etxarri, A.; Koh, A. L.; Dionne, J. A. Observation of Quantum Tunneling between Two Plasmonic Nanoparticles. *Nano Lett.* **2013**, *13*, 564−569.
(44) Kraus, W. A.; Schatz, G. C. Plasmon Resonance Broadening in Small Metal Particles. *J. Chem. Phys.* **1983**, *79*, 6130−6139.
(45) Zhang, W.; Govorov, A. O.; Bryant, G. W. Semiconductor-Metal Nanoparticle Molecules: Hybrid Excitons and the Nonlinear Fano Effect. *Phys. Rev. Lett.* **2006**, *97*, 146804.
(46) Zhang, W.; Govorov, A. O. Quantum theory of the nonlinear Fano effect in hybrid metal-semiconductor nanostructures: The case of strong nonlinearity. *Phys. Rev. B* **2011**, *84*, 081405.
(47) Trügler, A.; Hohenester, U. Strong coupling between a metallic nanoparticle and a single molecule. *Phys. Rev. B* **2008**, *77*, 115403.
(48) Ridolfo, A.; Stefano, O. D.; Fina, N.; Saija, R.; Savasta, S. Quantum Plasmonics with Quantum Dot-Metal Nanoparticle Molecules: Influence of the Fano Effect on Photon Statistics. *Phys. Rev. Lett.* **2010**, *105*, 263601.
(49) Morton, S. M.; Jensen, L. A Discrete Interaction Model/Quantum Mechanical Method for Describing Response Properties of Molecules Adsorbed on Metal Nanoparticles. *J. Chem. Phys.* **2010**, *133*, 074103.
(50) Waks, E.; Sridharan, D. Cavity QED treatment of interactions between a metal nanoparticle and a dipole emitter. *Phys. Rev. A* **2010**, *82*, 043845.
(51) Manjavacas, A.; de Abajo, F. J. G.; Nordlander, P. Quantum Plexcitonics: Strongly Interacting Plasmons and Excitons. *Nano Lett.* **2011**, *11*, 2318.
(52) Shah, R. A.; Scherer, N. F.; Pelton, M.; Gray, S. K. Ultrafast reversal of a Fano resonance in a plasmon-exciton system. *Phys. Rev. B* **2013**, *88*, 075411.
(53) Chen, X.-W.; Sandoghdar, V.; Agio, M. Coherent Interaction of Light with a Metallic Structure Coupled to a Single Quantum Emitter: From Superabsorption to Cloaking. *Phys. Rev. Lett.* **2013**, *110*, 153605.
(54) Sadeghi, S. M.; Hatef, A.; Meunier, M. Quantum detection and ranging using exciton-plasmon coupling in coherent Nanoantennas. *Appl. Phys. Lett.* **2013**, *102*, 203113.
(55) Zelinskyy, Y.; Zhang, Y.; May, V. Photoinduced dynamics in a molecule metal nanoparticle complex: Mean−field approximation

versus exact treatment of the interaction. *J. Chem. Phys.* **2013**, *138*, 114704.
(56) Hohenberg, P.; Kohn, W. Inhomogeneous Electron Gas. *Phys. Rev.* **1964**, *136*, B864−B871.
(57) Kohn, W.; Sham, L. J. Self-Consistent Equations Including Exchange and Correlation Effects. *Phys. Rev.* **1965**, *140*, A1133−A1138.
(58) Runge, E.; Gross, E. K. U. Density-Functional Theory for Time-Dependent Systems. *Phys. Rev. Lett.* **1984**, *52*, 997−1000.
(59) Dreizler, R. M.; Gross, E. K. U. *Density Functional Theory*; Springer: Berlin, 1990. Fiolhais, C.; Nogueira, F.; Marques, M., Eds. *A Primer in Density Functional Theory*; Springer: Berlin, 2003.
(60) Marques, M. A. L.; Ullrich, C. A.; Nogueira, F.; Rubio, A.; Burke, K.; Gross, E. K. U., Eds. *Time-Dependent Density Functional Theory*; Springer-Verlag: Berlin, 2006.
(61) Madelung, O. *Semiconductors: Data Handbook*, 3rd ed.; Springer: Berlin, 2004.
(62) Bohren, C. F.; Huffman, D. R. *Absorption and Scattering of Light by Small Particles*; John Wiley & Sons, Inc.: New York, 1983.
(63) Heitmann, D.; Kotthaus, J. P.; Mohr, E. G. Plasmon dispersion and intersubband resonance at high wavevectors in Si(100) inversion layers. *Solid State Commun.* **1982**, *44*, 715−718.
(64) Sooryakumar, R.; Pinczuk, A.; Gossard, A.; Wiegmann, W. Dispersion of collective intersubband excitations in semiconductor superlattices. *Phys. Rev. B* **1985**, *31*, 2578−2580.